Concatenated Modular BK Channel Constructs Reveal Divergent Stoichiometry in Gating Control by LRRC26 (γ1), Pore, and Selectivity Filter

Guanxing Chen, Qin Li, Kunal Shah, Jiusheng Yan*

[1]Department of Anesthesiology and Perioperative Medicine, The University of Texas MD Anderson Cancer Center, Houston, Texas, USA

*Correspondence:

Jiusheng Yan, Department of Anesthesiology and Perioperative Medicine, The University of Texas MD Anderson Cancer Center, Houston, Texas, USA

Email: jyan1@mdanderson.org

Abstract

Big-conductance, Ca^{2+}-activated K^+ (BK) channels consist of Ca^{2+}- and voltage-sensing, pore-forming α (BKα) subunits and regulatory auxiliary β or γ subunits. Concatenated subunit constructs are powerful tools for elucidating subunit stoichiometry in ion channel gating and regulation, allowing control over subunit arrangement, stoichiometry, and mutation. However, the additional S0 transmembrane segment in BKα places its N- and C-termini on opposite sides of the membrane, preventing tandem BK channel subunit construction by conventional methods. To investigate the atypical "all-or-none" modulatory function of γ subunits and the subunit stoichiometry of BK channel gating, we developed concatenated constructs containing 2 or 4 BKα subunits by splicing them into modular forms that can be co-expressed to form functional channels. These constructs retained voltage and Ca^{2+} gating properties similar to intact BK channels. By fusing the LRRC26 (γ1) subunit to the N-terminus of tandem BKα constructs, we found that a single γ1 subunit per α subunit tetramer is sufficient to fully modulate the channel. Furthermore, the L312A mutation in the deep pore region exhibited a stoichiometrically graded effect on voltage-gated BK channel activation. In contrast, a V288A mutation at the selectivity filter induced channel inactivation only when present in all four BKα subunits. Thus, by engineering concatenated BKα constructs, we identified three distinct stoichiometric modes of BK channel gating control by LRRC26, the pore, and the selectivity filter. This study offers new molecular tools and advances our understanding of subunit stoichiometry in BK channel gating and modulation.

Introduction

The big-conductance, calcium- and voltage-activated K^+ (BK) channel is a unique member of the potassium channel family, characterized by exceptionally large single-channel conductance and dual regulation by membrane voltage and intracellular free Ca^{2+} (1). The BK channel is a homotetramer composed of four identical pore-forming, Ca^{2+}- and voltage-sensing α (BKα) subunits (~130 kDa) and variable auxiliary subunits. BK channels exhibit prominent features in molecular architecture (2, 3) and allosteric gating mechanisms (4, 5). In the transmembrane (TM) domains, BK channels differ from most voltage-gated K^+ (Kv) channels by possessing an extra S0 TM helix, lacking domain swapping between the S1-S4 voltage-sensing domain (VSD) and the S5-S6 pore-gate domain (PGD), and exhibiting tight VSD-PGD packing via extensive S4-S5 interactions (2). The BKα subunit also contains a large cytosolic C-terminus composed of two tandem RCK domains (RCK1, RCK2) responsible for Ca^{2+} and Mg^{2+} sensing (5-11). The RCK domains from all BKα subunits assemble into a tetrameric two-layer gating ring that expands and shifts toward the membrane in response to Ca^{2+} bindings, leading to S6 movement and channel opening (8, 9).

BK channel function is regulated by auxiliary β and γ subunits and by LINGO1, conferring tissue-specific gating and pharmacological properties (12-18). The four γ subunits (γ1-γ4), also known as LRRC26, LRRC52, LRRC55, and LRRC38, are leucine-rich repeat (LRR)-containing membrane proteins (15, 16). The γ subunits facilitate BK channel activation by shifting the voltage dependence of channel activation in the hyperpolarizing direction by ~140 mV (γ1), 100 mV (γ2), 50 mV (γ3), and 20 mV (γ4), in terms of half-maximal activation voltage ($V_{1/2}$) in the absence of Ca^{2+}. The γ1 subunit likely modulates BK channels by enhancing the allosteric coupling between VSD activation and the pore opening (15). All γ subunits share a common topology, including an N-terminal signal peptide, an extracellular LRR domain, a single TM segment, and a short intracellular C-terminus (15, 16, 19). Their modulatory effects on BK channel voltage gating are mainly determined by the TM segments and C-terminal clusters of positively charged residues (20, 21), while the LRR domains regulate the γ subunits' expression and surface trafficking (19). Recent cryo-EM structures of BKα/γ1 complexes show that the LRRC26's TM segment binds peripherally to the BKα VSD, involving S0, S2, S3, and pre-S1 helices, while the LRR domains tetramerizes extracellularly without directly contacting BKα (22-24).

A fundamental question in ion channel gating and regulation is the structural and functional subunit stoichiometry. BK channel modulation by the γ subunits exhibits an atypical binary "all-or-none" phenotype: voltage-dependence ($V_{1/2}$) is either fully shifted or unchanged under limited γ1 expression (19,

25). In tetrameric ion channels, auxiliary proteins typically follow 4-fold symmetry, producing graded modulation based on subunit stoichiometry relative to the pore-forming principal subunit, as observed with BK β subunits (26), KCNE subunits on KCNQ channels (27), and KChIP subunits on Kv4 channels (28). Consistent with previous reports detecting up to four γ1 subunits per channel (29-31), Cryo-EM structures also show a symmetric presence of four γ1 subunits in BKα/γ1 complexes (22-24). However, single-channel recordings using a β2-γ1 chimeric subunit suggest that even a single γ1 subunit is sufficient for full modulation (29). It is of note that the evidence remains inconclusive due to several limitations: the chimeric construct lacks the LRR domain, which may influence γ1 function (19); the inferred subunit number is indirectly based on the β2 N-terminal blockade effect; and the sample size in number of channels is limited by the single-channel recording method. Moreover, given the largely independent impact of the individual VSDs to BK channel gating (4) and the symmetric presence of γ1 near all VSDs (22-24), an alternative concerted "all-subunits-required" model, involving extracellular LRR domain tetramerization, has been proposed (22). Therefore, direct biochemical determination of the functional stoichiometry of γ1 in BK channel modulation is needed.

Concatenated subunit constructs with 2 or 4 channel subunits fused together in a C-to-N-terminal arrangement have been powerful tools for dissecting subunit stoichiometry and cooperativity in various voltage- and/or ligand-gated channels (32-38). However, the additional S0 segment in BKα prevents straightforward concatenation, as its N- and C-termini reside on opposite sides of the membrane. BK channels, owing to their unique biophysical properties, serve as a value model for studying allosteric gating mechanisms of multimodal ion channels (4). Yet, the unavailability of functional BKα concatemers has hindered precise stoichiometric investigations of channel gating and modulation at both intra- and inter-subunit levels.

To address this, we engineered modular BKα constructs that reassemble into functional concatenated channels with biophysical properties comparable to intact BK channels. Using these, we demonstrate that a single γ1 subunit per BKα tetramer is sufficient to fully modulate the channel. Given the central role of the PGD in BK channel gating, we further applied this system to mutational analyses of the deep pore and selectivity filter. We revealed distinct stoichiometric requirements for gating control by LRRC26, the pore, and the selectivity filter. This study provides new molecular tools and mechanistic insights into the stoichiometry of BK channel gating and regulation.

Results

Construction of functional BK channels with concatenated tandem repeats of the α subunits

We employed multiple strategies to generate concatenated BKα subunit constructs that enable expression of functional channels with biophysical properties that are comparable to intact (i.e., unsplit) BK channels and facile amplification and manipulation at the plasmid DNA level. Given the extracellular location of the N-terminus of BKα (Fig. 1A), which precludes direct C-to-N-terminal concatenation, we first attempted to split BKα into the N-terminal S0 part and the remaining major portion. This was based on the report that co-expression of these two parts can form functional channels (39). However, plasmids of tandem constructs lacking only S0 proved difficult to generate and use due to large plasmid size and instability during cloning. Since the C-terminal RCK2 domain can also be expressed as a module that forms functional channels when split and co-expressed with the rest of BKα (40), we thus further split BKα into a main part (residues 94-649), designated as α_M, and the rest by deletion of the main part, designated as $\alpha^{\Delta M}$ (Fig. 1A, B). The α_M module contains the major transmembrane region (S1 to S6) and the RCK1 domain. The $\alpha^{\Delta M}$ construct retains the N-terminal residues 1-93 including S0 and the C-terminal residues 652-1113 including the RCK2 domain.

To prevent homologous recombination within the concatenated tandem repeat constructs during molecular cloning and to facilitate site-directed mutations on specific subunits, we designed each BKα subunit in the repeats to have distinct DNA sequences. This was achieved by utilizing codon-optimized cDNA sequences for the 2nd, 3rd, and 4th repeats of the main part, which differ by ~ 25% in nucleotide sequence from the original 1st repeat and from each other. With these strategies, we generated a single unit and tandem constructs of double and quadruple repeats of α_M, named $\alpha_{M(mono)}$ (α_M), $\alpha_{M(dual)}$ (α_{MM}), and $\alpha_{M(quad)}$ (α_{MMMM}), respectively (Fig. 1B). To evaluate the expression and stability of the concatenated tandem α_M constructs, we performed immunoblot analysis of the C-terminally V5-tagged constructs transfected in HEK293 cells. The result showed predominant protein bands of α_{MM} and α_{MMMM} at expected protein sizes recognized by the anti-V5 antibody (Fig. 1C), confirming the expression and lack of major degradation of the concatenated α_M constructs. The expression level of the $\alpha^{\Delta M}$ construct was affected by the α_M construct and co-immunoprecipitation confirmed the complex formation between the α_M and $\alpha^{\Delta M}$ constructs (Fig. 1 - figure supplement 1).

By co-expression of the C-terminally GFP-tagged $\alpha^{\Delta M}$ ($\alpha^{\Delta M}$-GFP) with single, double, or quadruple repeat constructs of α_M, we observed formation of functional BK channels that resemble the intact BKα channel in their voltage and Ca^{2+}-dependence of channel activation (Fig. 1D, E). The $V_{1/2}$

values of the BK channels formed by the single-unit α_M construct, when co-expressed with $\alpha^{\Delta M}$-GFP, were 192 and 16 mV at virtual 0 and 10 μM Ca^{2+}, respectively. The tandem double repeat constructs, α_{MM}, when co-expressed with $\alpha^{\Delta M}$-GFP, produced functional BK channels with $V_{1/2}$ values of 186 mV at virtual 0 Ca^{2+}, and 16 mV at 10 μM Ca^{2+} (Fig. 1E; Table 1). Furthermore, the channels formed by tandem quadruple repeat construct α_{MMMM} and $\alpha^{\Delta M}$-GFP had $V_{1/2}$ values of 184 and 29 mV at virtual 0 and 10 μM Ca^{2+}, respectively (Fig. 1E; Table 1). These $V_{1/2}$ values of engineered BK channels formed by single, double, and quadruple repeat constructs of α_M are close to those of the intact BKα channels, which had $V_{1/2}$ = 172 and 19 mV at virtual 0 and 10 μM Ca^{2+}, respectively (Table 1). These results show that the voltage- and Ca^{2+}-gating properties are largely unaltered in the engineered BK channels formed by engineered concatenated BKα subunit constructs.

A single LRRC26 (γ1) subunit per channel is sufficient to fully modulate BK channels

The γ1 subunit's "all-or-none" modulatory effect on BK channels has remained mechanistically elusive, despite the recent availability of 3D structures of the BKα/γ1 complexes. To directly investigate the functional stoichiometry of BK channel modulation by the γ1 subunit, we fused the C-terminus of the γ1 subunit to the N-terminus of the first α_M repeat in the α_{MM} and α_{MMMM} constructs, generating the BKγ1α_{MM} (BKγ1$\alpha_{M(dual)}$) and BKγ1α_{MMMM} (BKγ1$\alpha_{M(quad)}$) fusion constructs (Fig. 2B). Immunoblot analysis of the V5-tagged constructs using an anti-V5 antibody showed a major band at the expected size for both BKγ1α_{MM} (~150 kDa) and BKγ1α_{MMMM} (~270 kDa) (Fig. 2C), confirming proper expression and stability. Upon co-expression of these constructs with $\alpha^{\Delta M}$-GFP in HEK293 cells, we observed that the N-terminally fused γ1 subunit induced a $V_{1/2}$ shift of 125 mV with the BKγ1α_{MM} construct ($V_{1/2}$ = 62 ± 5 mV) and 145 mV with the BKγ1α_{MMMM} construct ($V_{1/2}$ = 38 ± 4 mV) in the virtual absence of Ca^{2+} (Fig. 2D, E). These large $V_{1/2}$-shifting effects in stoichiometrically defined γ1:α = 1:2 and 1:4 channel complexes clearly indicate that a single γ1 subunit per tetrameric channel is sufficient to fully modulate BK channels. This "one-subunit-sufficient" effect provides a mechanistic explanation for the observed binary, all-or-none modulation by the γ1 subunit when its expression is limited.

L312A mutation reveals stoichiometrically graded gating and confirms functional integrity of concatenated constructs

To ensure that the concatenated α_M constructs are suitable for studying the stoichiometry of BK channel gating and regulation, the constructs must demonstrate two additional aspects of functional integrity

beyond simply forming functional channels. First, each α_M repeat within the construct should contribute equally to channel formation. Second, the concatenated dual and quadruple α_M repeats in the $\alpha_{M(dual)}$ and $\alpha_{M(quad)}$ constructs should assemble primarily as complete units, i.e., two $\alpha_{M(dual)}$ constructs or one $\alpha_{M(quad)}$ construct should form a single channel. The latter ensures that heterogeneous channels with uncontrolled subunit stoichiometry are unlikely to form and confound the results.

To evaluate the functional integrity of the concatenated constructs and to examine the stoichiometry of activation gating in the PGD, we investigated the mutational effects of the deep pore residue L312 (^{307}FILGGLAMFAS^{317}) (Fig. 3A), which plays a pivotal role in BK channel activation gating. Most mutations at this site resulted in constitutively active channels (41). The L312A mutation, in particular, causes a substantial shift of the $V_{1/2}$ toward hyperpolarization potentials in the absence of Ca^{2+} (41, 42). We first confirmed that the L312A mutation on the single-repeat α_M construct caused a similarly large (~130 mV) shift in $V_{1/2}$ toward hyperpolarization in Ca^{2+}-free conditions (Fig. 3B, C; Table 1). We then introduced the L312A mutation into the dual- and quadruple-repeat α_{MM} and α_{MMMM} constructs in a repeat-specific manner. For the α_{MM} construct, introducing L312A mutation into either the first or second repeat resulted in a similar shift (65 or 68 mV) in $V_{1/2}$, approximately half of the total shift seen when both repeats (i.e., all subunits) were mutated (Fig. 3C; Table 1). For the α_{MMMM} construct, we observed that the voltage dependence of the channel activation shifted progressively with each additional L312A mutation introduced. Specifically, the initial L312A mutation on the first repeat shifted $V_{1/2}$ by 31 mV, with further increases of 20, 35, and 37 mV in $V_{1/2}$ shifts observed for the additional mutation on the second, third, and fourth repeats, respectively (Fig. 3D; Table 1). The L312A mutation also caused a slowed decay in tail currents at negative voltages (Fig. 3B) compared to unmutated channels (Fig. 1D). Fitting the current decay kinetics revealed that the time constant (τ) of the decay was increased with the number of L312A mutations present in the channels formed by α_{MM} and α_{MMMM} constructs (Fig. 1E). It is worth noting that the tail current decay rates for channels with zero or one L312A mutation were likely overestimated due to rapid closure at very negative voltages (-120 mV) in Ca^{2+}-free conditions, exceeding the detection limit of the 2 kHz-filtered recordings. These results demonstrate a stoichiometrically incremental effect of the L312A mutation on BK channel voltage gating. Importantly, they also indicate that individual BKα_M repeats in both the dual- and quadruple-repeat constructs contribute similarly to the gating properties of the assembled channels.

The conductance-voltage (G-V) curves of BK channels formed by these L312A mutant constructs were well-fit by a single Boltzmann function, with slopes (i.e., apparent gating charge z) remaining within

the typical range (Fig. 3C, D; Table 1), consistent with a largely homogenous channel population. In contrast, G-V curves of the channels formed by co-transfecting cells with WT and L312A single BKα subunit constructs (1:1 DNA ratio) showed shallow slopes (Fig. 3F), agreeing with the predicted heterogeneity in subunit composition and $V_{1/2}$ values. To confirm that each $\alpha_{M(quad)}$ construct predominantly forms a single channel without subunit exchange, we co-expressed fully mutated $\alpha_M{}^{L312A}{}_M{}^{L312A}{}_M{}^{L312A}{}_M{}^{L312A}$ and unmutated $\alpha_M{}^{WT}{}_M{}^{WT}{}_M{}^{WT}{}_M{}^{WT}$ constructs (1:1 DNA ratio). The resulting G-V curves were best fit with a double-Boltzmann function showing $V_{1/2}$ values matching those of the all-WT and all-L312A channels (Fig. 3F; Table 1). Additionally, tail currents at -120 mV exhibited two distinct exponential decay components differing by ~10-fold in rate, corresponding to populations of all-WT and all-mutated channels (Fig. 2G). These findings support that the concatenated α_M repeats in the $\alpha_{M(dual)}$ and $\alpha_{M(quad)}$ constructs function as a whole unit in channel assembly, enabling stoichiometrically defined investigation of channel gating and regulation.

V288A triggers selectivity filter inactivation through an all-subunit mechanism

The selectivity filter in K^+ channels is directly involved in C-type inactivation. Given its potential role in BK channel activation gating (43, 44), we examined the subunit stoichiometric effects of structural perturbations within the selectivity filter on BK channel gating. We found that the V288A mutation, located within the K^+-selective signature sequence (^{286}ST<u>V</u>GYGD^{292}) (Fig. 3A), produced profound effects on BK channel gating. We previously reported that mutations near the selectivity filter, e.g., in the P-helix (Y279) or at the extracellular side of the filter (Y294), can induce an atypical closed-state-coupled C-type inactivation in BK channels under low extracellular K^+ conditions (44). Interestingly, V288A, even without reduced extracellular K^+, induced a similar slow inactivation process, causing a gradual decrease in the availability of activatable channels under conditions (e.g., negative voltages) that promote channel closure (Fig. 4A). Consequently, compared to WT channels, V288A mutant channel currents developed very slowly in response to depolarization (Fig. 4B**)**. However, following a long pre-depolarization, the mutant channels fully recovered from the inactivated state and behaved similarly to WT channels in the kinetics and voltage-dependence of activation (Fig. 4C).

Using the concatenated BKα_M constructs, we investigated the subunit stoichiometry of V288A-induced gating effects by introducing the mutation into different numbers of BKα subunits within a single channel. With the BK$\alpha_{M(dual)}$ construct, we generated $\alpha_M{}^{V288A}{}_M{}^{WT}$ and $\alpha_M{}^{V288A}{}_M{}^{V288A}$ constructs, harboring the mutation on half or all subunits, respectively. We introduced one ($\alpha_M{}^{V288A}{}_M{}^{WT}{}_M{}^{WT}{}_M{}^{WT}$), two

($\alpha_M^{V288A}{}_M^{V288A}{}_M^{WT}{}_M^{WT}$), three ($\alpha_M^{V288A}{}_M^{V288A}{}_M^{WT}{}_M^{V288A}$), or four ($\alpha_M^{V288A}{}_M^{V288A}{}_M^{V288A}{}_M^{V288A}$) mutations on the BK$\alpha_{M(quad)}$ construct. Interestingly, unlike the one-subunit-sufficient effect of LRRC26 or the stoichiometrically incremental effects of the L312A mutation, V288A exerted an "all-subunit-required" modulatory effect: the V288A-induced changes occurred only when all four BKα subunits in a channel were mutated. Channels partially mutated, originated from $\alpha_M^{V288A}{}_M^{WT}$, $\alpha_M^{V288A}{}_M^{WT}{}_M^{WT}{}_M^{WT}$, $\alpha_M^{V288A}{}_M^{V288A}{}_M^{WT}{}_M^{WT}$, or $\alpha_M^{V288A}{}_M^{V288A}{}_M^{WT}{}_M^{V288A}$, showed no significant differences from WT channels in the time course (Fig. 4D, E) or voltage-dependence (Fig. 4F) of depolarization-induced currents. In contrast, channels with all α_M repeats mutated ($\alpha_M^{V288A}{}_M^{V288A}$ and $\alpha_M^{V288A}{}_M^{V288A}{}_M^{V288A}{}_M^{V288A}$) displayed markedly slowed current development, approximately 100-fold slower than WT (Fig. 4D, E). These fully mutated channels also showed an apparently higher $V_{1/2}$ in their G-V relationships (Fig. 4F). However, since the V288A mutation has no significant effect on the channel's normal activation gating (Fig. 4C, F), this apparent shift in G-V curves likely resulted from incomplete recovery of inactivated channels during 50 ms depolarization phase in the voltage protocol used. Together, these results demonstrate that V288A induces an "all-subunit-required" inactivation process at the selectivity filter, while the activation/deactivation processes of normal channel gating remain largely unchanged.

Discussion

Concatenated constructs have been extensively used to study ion channel subunit stoichiometry (32-38), enabling a deeper understanding of the mechanisms underlying channel gating and regulation by homo- or heteromeric subunits, voltage, ligands, and mutations. However, the BK channel is one of the few channels whose principal subunits have their N-termini located on the extracellular side. This unique membrane topology prevents the direct application of the traditional N-to-C-terminal concatenation method for generating the concatenated constructs. In this study, we employed a strategy that involved splitting and fusing BKα subunits into two modular constructs that reconstitute functional BK channels. We validated the functionality of these concatenated constructs by demonstrating that the resulting channels closely resemble intact BK channels in their voltage and Ca^{2+} dependence of activation. Furthermore, we confirmed that each repeat with the constructs contributes similarly to channel function, as evidenced by the stoichiometrically incremental effect of the L312A mutation on voltage gating. Previous studies have reported that, in some cases, subunits from different quadruple-repeat concatemers can assemble aberrantly, leading to the formation of mixed channels with altered properties (45, 46). The large functional effect of the L312A mutation on BK channel gating allowed us to distinguish between

properly assembled channels and potential inter-subunit crossover products. Our results showed that the concatenated tandem constructs assemble predominantly as intended, i.e., each channel is formed by two dual-repeat constructs or a single quadruple-repeat construct, as evidenced by the absence of significant heterogeneity in channel gating properties. Using these well-defined concatenated constructs, we identified three distinct types of subunit stoichiometry in BK channel gating or modulation. These rule out the possibility that the observed stoichiometric effects are artifacts arising from the construct design or assembly defects. Thus, we have demonstrated that our engineered concatenated BKα constructs serve as effective molecular tools for probing the subunit stoichiometry in BK channel gating and regulation.

Most auxiliary proteins of the K^+ channels exhibit stoichiometrically incremental effects on channel modulation. However, the auxiliary γ1 subunit displays an unusual binary "all-or-none" modulatory effect on BK channels (19, 25), despite being able to bind to BKα subunits at a 1:1 molecular ratio (29-31). In recently reported cryo-EM structures of channel complexes, the four γ1 subunits display an apparent four-fold symmetry in TM domain interactions with their LRR domains tetramerized on the extracellular side (22-24). These structural features raise the possibility that the four γ1 subunits might act collectively in BK channel modulation (22), which appears to contradict the "one-subunit-sufficient" mechanism previously inferred from single channel gating properties of BK channels modulated by a β2-γ1 chimeric construct (29). With the concatenated modular BKα constructs developed in this study, we were able to directly control the subunit stoichiometry of γ1 subunits relative to BKα subunits. The intracellular location of the N-terminus in the concatenated BKα constructs enabled us to fuse the γ1 subunit to the N-terminal side of the α_M module. With γ1-fused concatenated α_M dual- and quadruple-repeat constructs, we provide direct evidence that one and two copies of the γ1 subunits per BKα tetramer are sufficient to produce the full modulatory effect of the γ1 subunit on BK channel gating. Thus, our findings unequivocally confirm the "one-subunit-sufficient" mechanism of the γ1 subunit in BK channel modulation by using the full length γ1 subunit, stoichiometrically defined BKα/γ1 channel complexes, and macroscopic currents from large channel populations. This result, combined with the structural observation of symmetrical binding of γ1 to all four voltage-sensor domains, raises the intriguing possibility that γ1 modulation may occur through asymmetric allosteric coupling, despite symmetric structural binding—a phenomenon warranting further mechanistic investigation.

Through conformational linkage to the voltage- and Ca^{2+}-sensors, the movement of the lower half of the pore-lining S6 helix ultimately controls BK channel pore gating. According to the Horrigan-Aldrich gating model (4), BK channel activation involves a rate-limiting process of pore-gate opening, regulated

by four independent and identical voltage- and Ca^{2+}-sensors. However, the subunit stoichiometry underlying the S6 movement-induced pore-gate opening in BK channels remains unclear and warrants investigation. The deep pore residue L312 on S6 is unique in that it lies adjacent to the double-glycine gating hinge residues (G310 and G311), is positioned immediately below the selectivity filter (Fig. 3A), and appears to be the most mutation-sensitive residue affecting channel activation gating, as most of its substitution mutations result in constitutively open channels (41). Thus, L312 appears to represent a structural endpoint for the voltage- and Ca^{2+}-induced conformational changes in S6 and plays an essential role in stabilizing the channel's closed state. In classic Shaker K^+ channels, a mutation of the neighboring glycine hinge residue (G466 in Shaker, corresponding to G311 in BKα) in concatenated tetrameric constructs was reported to display a concerted, "one-subunit-sufficient" effect, where all mutant subunit combinations produced similar effects on channel gating (37), a phenomenon reminiscent of the modulatory behavior of the LRRC26 (γ1) subunit on BK channel gating. In contrast, our current study reveals a stoichiometrically graded (independent) effect of the L312A mutation on BK channel voltage gating. Similarly, single channel recordings showed that a mutation to arginine at the neighboring G311 residue also produced an additive effect on the BK channel voltage-gating proportional to the number of mutated subunits (47). Together, the observed stoichiometric independence of mutational effects at the L312 and G311 residues is consistent with the modeled independence of individual voltage and Ca^{2+} sensors in channel activation (4, 47), and likely reflects a fundamental difference in the location and mechanism of the activation gate. Currently, the fundamental question of pore gate location in BK channels remains unsettled. In most K^+ channels, a hydrophobic "bundle-crossing" gate near the intracellular end of the pore controls channel activation (48). However, BK channels appear to lack such a gate, as the pore remains structurally wide open in the presumed closed-state (Ca^{2+}-free) structures (2, 8) and is readily accessible to large intracellular blockers (49, 50) or cysteine-modifying reagents (51) even when the channel is closed. Thus, in Shaker and related Kv channels, the classical activation gate resides within the lower S6 helices, where concerted subunit movements are required for highly cooperative transitions from closed to open states. In contrast, the graded, additive effects of deep pore mutations in BK channels provide evidence that no such concerted gating structure exists within the lower S6 or at least not within the deep pore region.

The selectivity filter, known to govern C-type inactivation in many channels (52-54), may also serve as activation gate in some, such as the ligand-gated CNG channels (55). Accordingly, direct involvement of the selectivity filter in BK channel activation gating has long been speculated (34, 43, 49),

but compelling experimental validation remains lacking. While C-type inactivation doesn't normally occur in BK channels, we previously found that it can be induced by mutations near the selectivity filter in combination with low extracellular K^+ (44). Interestingly, the induced C-type inactivation in BK channels is closed-state coupled (44), opposite to the open-state coupled C-type inactivation commonly observed in other channels. In this study, we report that the V288A mutation, located within the K^+-selective signature sequence, also induces pronounced inactivation even under normal extracellular K^+ conditions. Our analysis of the subunit stoichiometric effects of V288A using concatenated BKα dual- and quadruple-repeat constructs clearly showed that modifications in all four subunits are required to elicit the mutation-induced inactivation, whereas all other mutant subunit combinations produced minimal effects on BK channel gating. It is noteworthy that the stoichiometric effects of mutations on the rate of C-inactivation varies depending on the location of the mutated residue in other voltage-gated K^+ channels. Mutations located more peripherally from the selectivity filter signature motif often produced either a non-linear, graded effect consistent with a cooperative inter-subunit interaction (e.g., A463V, A449K, and W434F in Shaker channels, or S631A and T618A in hERG1) (36, 38, 56), or a linearly additive effect consistent with inter-subunit independence (e.g., M645C in hERG1) (38). In contrast, mutations near or within the selectivity filter signature motif affected C-type inactivation in an all-or-none manner, with a single subunit mutation, such as S620T or G628C in hERG1, being sufficient to eliminate or attenuate inactivation to the same extent as observed in mutant homotetramers (38). This effect closely mirrors our observations with V288A in BK channels, where mutations in all four subunits are required to induce and maintain inactivation, supporting our interpretation that V288A induces a form of C-type inactivation, similar to what we previously observed with mutations at the extracellular mouth and the P-helix (44). Given its critical location, the V288A mutation may alter BK channel ion selectivity, as an alanine substitution at the equivalent position in Kv4.3 has been shown to reduce K^+ selectivity (57). Whether V288A induces both C-type inactivation and changes in ion selectivity through a similar subunit stoichiometry remains to be determined.

The contrasting behaviors of L312A and V288A mutations in concatenated BK α_M constructs reveal distinct subunit stoichiometry requirements between the deep pore activation gating and selectivity filter inactivation gating. A typical K^+ channel activation gate requires all four subunits undergo a concerted conformational change to ensure an all-or-none transition between a fully conductive and non-conductive pore (58, 59), a hallmark of classic voltage-gated K^+ channels that allows rapid and precise control of membrane excitability. Such tight inter-subunit all-or-none cooperativity observed at the BK

channel selectivity filter makes it a plausible candidate for serving as the activation gate, a property not yet demonstrated for the lower S6 segment. It is possible that the selectivity filter functions as the physical gate for two gating processes, activation and inactivation, that can occur on different timescales and through distinct structural mechanisms. Previously, we found that the voltage- and Ca^{2+}-dependence of inactivation and activating gating were well correlated in BK channels (44), suggesting a shared or coupled energetic pathway. L312 lies in close proximity to and physically interacts with the selectivity filter, providing a possible structural link for transmitting energy from S6 movement to the selectivity filter during activation gating. Further investigation of inactivation and its relationship to activation will likely help elucidate the role of the selectivity filter in BK channel activation gating.

In conclusion, our study employed an innovative strategy to generate concatenated subunit constructs and investigate the subunit stoichiometry and modulation of BK channels. The development of these constructs enabled detailed exploration of the intricate gating and regulatory mechanisms of BK channels in a stoichiometrically subunit-specific manner. Using these concatenated constructs, we identified three distinct types of subunit stoichiometry in BK channel modulation: an additive (independent) type and two contrasting all-or-none types, namely, "one-subunit-sufficient" and "all-subunit-required". These represent divergent stoichiometric modes of gating control by the pore, LRRC26 (γ1), and selectivity filter, respectively. This study offers new molecular tools and advances our understanding of subunit stoichiometry in BK channel gating and modulation.

Materials and Methods

Generation of concatenated tandem BKα repeat constructs and expression of BK channels

We first generated a pcDNA6-based plasmid, pcDNA6-myc-BKα-V5-His, carrying *KCNMA1* cDNA (GenBank: U11058). This plasmid expresses the full-length (1113 amino acids) human BKα (GenBank: AAB65837) with an N-terminal Myc tag and C-terminal V5 and 6×His tags, serving as the template for further plasmid constructions. To express BKα's main region (residues 44-651) as a protein module, we created pcDNA6-myc-α_M-V5-His by deleting the nucleotide sequences encoding N-terminal residues 1-43 (extracellular N-terminus and S0 TM segment) and C-terminal residues 652-1113 (RCK2 domain and C-terminal tail). Next, we constructed a complementary plasmid, pcDNA6-myc-BK$\alpha^{\Delta M}$-GFP-V5-His, by replacing residues 94-651 of BKα with a flexible peptide linker (SSGGGGSGGGSGGAR) and tagging monomeric enhanced GFP to the C-terminus. This complementary plasmid enables functional channel formation when co-expressed with a plasmid encoding a single α_M or concatenated α_M repeats. To

construct structurally stable plasmids expressing concatenated α_M repeats, we synthesized three codon-optimized DNA sequences encoding the same α_M module, each differing by ~ 25% in nucleotide sequence from each other and the original *KCNMA1* cDNA. Using these synthesized sequences, we constructed the dual-repeat expressing plasmid, pcDNA6-$\alpha_{M1}\alpha_{M2}$-V5-His, in which α_{M1} (residues 43-649) is preceded by a short initiation sequence (MGS) and linked to α_{M2} (also residues 43-649) via a flexible linker (GGGGSGSAG). A NotI restriction site with a peptide spacer (GGGKPIPNAAA) was inserted between α_{M2} and the V5 tag. We also generated a second dual-repeat expressing plasmid, the pcDNA6-$\alpha_{M3}\alpha_{M4}$-V5-His, in which α_{M3} (residues 44-649) is preceded by an N-terminal sequence (MGAAAA) containing a NotI site and linked α_{M4} (residues 43-649) via a flexible linker (GGGSAAGSG). As the two dual-repeat constructs produce highly similar proteins and exhibit no difference in electrophysiological properties, both are referred to as BK$\alpha_{(dual)}$ or α_{MM}. To generate a quadruple-repeat expressing plasmid, pcDNA6-$\alpha_{M1}\alpha_{M2}\alpha_{M3}\alpha_{M4}$-V5-His, we subcloned the $\alpha_{M3}\alpha_{M4}$ dual-module fragment from pcDNA6-$\alpha_{M3}\alpha_{M4}$-V5-His into pcDNA6-$\alpha_{M1}\alpha_{M2}$-V5-His using NotI and AgeI (located between the V5 and 6×His tags). The expressed protein is referred as BK$\alpha_{(quad)}$ or α_{MMMM}. For γ1 (LRRC26) fusion constructs, we generated pcDNA6-BKγ1$\alpha_{M1}\alpha_{M2}$-V5-His and by inserting the γ1 (LRRC26) sequence at the N-terminus of $\alpha_{M1}\alpha_{M2}$ (pcDNA6-$\alpha_{M1}\alpha_{M2}$-V5-His) via a 16-residue flexible linker (SSGSGSESKSTGGSGS). The expressed fusion protein is designated as BKγ1α_{MM} or BKγ1$\alpha_{M(dual)}$. To express the BKγ1α_{MMMM} (also referred as BKγ1$\alpha_{M(quad)}$) fusion construct, we created pcDNA6-BKγ1$\alpha_{M1}\alpha_{M2}\alpha_{M3}\alpha_{M4}$-V5-His by subcloning $\alpha_{M3}\alpha_{M4}$ from pcDNA6-$\alpha_{M3}\alpha_{M4}$-V5-His into pcDNA6-BKγ1$\alpha_{M1}\alpha_{M2}$-V5-His using NotI and AgeI. For DNA manipulation and amplification, we used the Long Fragment DNA Ligation Kit (TaKaRa) and CopyCutter competent E. coli (Lucigen). Site-directed mutagenesis was performed using the QuickChange kit (Stratagene). Mutations for the quadruple-repeat construct were first introduced into either the $\alpha_{M1}\alpha_{M2}$ or $\alpha_{M3}\alpha_{M4}$ dual-repeat construct, followed by fusion of $\alpha_{M1}\alpha_{M2}$ and $\alpha_{M3}\alpha_{M4}$ as described above. HEK293 cells were cultured in DMEM supplemented with 10% fetal bovine serum at 5% CO_2. Cells were transfected with plasmids using PEI "MAX" (Polysciences Inc.) and subjected to electrophysiological assays 16-72 hours post-transfection.

Electrophysiology

BK channel currents were recorded from excised inside-out patches of HEK293 cells using patch-clamp recording techniques as described previously (60). Both intracellular and extracellular (pipette) solutions contained 136 mM $KMeSO_3$, 4 mM KCl, and 20 mM HEPES (pH 7.20). The extracellular solution was

supplemented with 2 mM $MgCl_2$, while the intracellular solution contained 5 mM HEDTA either with or without Ca^{2+} to achieve 10 µM Ca^{2+} or Ca^{2+}free. Recording pipette electrodes were pulled from borosilicate filamented glass tubes (Cat #: BF150-110-10, Sutter Instrument) with a P-1000 micropipette puller (Sutter Instrument), and polished by heat with an MF-830 microforge (Narishige) to a resistance of 1-2 MΩ. Data were acquired using PatchMaster (HEKA) with an Axopatch 200B amplifier (Molecular Devices) and ITC-18 digitizer (InstruTECH) or with an EPC-10 amplifier (HEKA). Data were sampled at 20 µs and filtered at 2 kHz (Axopatch 200B) with the amplifiers' 4-pole Bessel filter or at 2.9 kHz (EPC-10). Time interval between voltage protocol sweeps was 2 s. Capacitive and leak currents were subtracted using a P/4 protocol at holding potentials of -120 mV or -150 mV (for γ1 or 10 µM Ca^{2+} conditions). Steady-state activation, expressed as normalized conductance (G/Gmax) versus voltage (G-V), was calculated from the tail current amplitudes (at -120 mV) and fitted using a single-Boltzmann function $G/Gmax= 1/(1+e^{-ZF(V-VH)/RT})$ or a double-Boltzmann function $G/Gmax = Pa/(1+ e^{-ZaF(V-VHa)/RT}) + (1 - Pa)/(1 + e^{-ZbF(V-VHb)/RT})$ where V, VH, Z, F, R, T, Pa, a and b denote voltage, $V_{1/2}$, gating charge (z), Faraday constant, gas constant, Kelvin temperature, component portion (0-1), and component identity (a or b), respectively. Values are reported as means ± SEM.

Immunoblotting

Proteins were enriched by immunoprecipitation as previously described (19) and immunoblotted after SDS-PAGE. Briefly, proteins were solubilized from cells in 2% Dodecyl-beta-D-maltoside (DDM) in TBS buffer (50 mM Tris, 150 mM NaCl, pH 7.6). Lysates were incubated with mouse anti-V5 monoclonal antibody agarose gel (Cat# A7345, Millipore Sigma) at 4 °C for 2 h. After three 10 min washes in with 2% DDM-containing TBS, bound proteins were eluted with 4% SDS. Protease inhibitor cocktail (Roche) was used throughout the procedure. Eluted proteins were separated by 4% to 20% gradient SDS-PAGE and transferred to PVDF membranes. Immunoblotting was performed with mouse anti-V5 monoclonal antibody (Cat# R96125, Invitrogen) at 1:10,000 dilution.

Data Availability

All relevant data are available in the published article.

Acknowledgement

This work was supported by National Institutes of Health grants NS078152 (J.Y.) and GM127332 (J.Y.).

Author Contribution

G.C., Q.L., and J.Y. designed experiments and analyzed data. G.C., Q.L., and K.S. performed experiments. G.C. and J.Y. wrote the manuscript.

Conflict of Interest

The authors declare no conflict of interests.

References

1. L. Salkoff, A. Butler, G. Ferreira, C. Santi, A. Wei, High-conductance potassium channels of the SLO family. *Nat. Rev. Neurosci.* **7**, 921-931 (2006).
2. X. Tao, R. MacKinnon, Molecular structures of the human Slo1 K(+) channel in complex with beta4. *eLife* **8** (2019).
3. X. Tao, C. Zhao, R. MacKinnon, Membrane protein isolation and structure determination in cell-derived membrane vesicles. *Proc Natl Acad Sci U S A* **120**, e2302325120 (2023).
4. F. T. Horrigan, R. W. Aldrich, Coupling between voltage sensor activation, Ca2+ binding and channel opening in large conductance (BK) potassium channels. *J Gen Physiol* **120**, 267-305 (2002).
5. X. M. Xia, X. Zeng, C. J. Lingle, Multiple regulatory sites in large-conductance calcium-activated potassium channels. *Nature* **418**, 880-884 (2002).
6. H. Yang, G. Zhang, J. Cui, BK channels: multiple sensors, one activation gate. *Frontiers in physiology* **6**, 29 (2015).
7. Y. Wu, Y. Yang, S. Ye, Y. Jiang, Structure of the gating ring from the human large-conductance Ca(2+)-gated K(+) channel. *Nature* **466**, 393-397 (2010).
8. R. K. Hite, X. Tao, R. MacKinnon, Structural basis for gating the high-conductance Ca2+-activated K+ channel. *Nature* **541**, 52-57 (2017).
9. X. Tao, R. K. Hite, R. MacKinnon, Cryo-EM structure of the open high-conductance Ca2+-activated K+ channel. *Nature* **541**, 46-51 (2017).
10. J. Shi *et al.*, Mechanism of magnesium activation of calcium-activated potassium channels. *Nature* **418**, 876-880 (2002).
11. T. Yusifov, N. Savalli, C. S. Gandhi, M. Ottolia, R. Olcese, The RCK2 domain of the human BKCa channel is a calcium sensor. *Proc Natl Acad Sci U S A* **105**, 376-381 (2008).
12. C. R. Solaro, C. J. Lingle, Trypsin-sensitive, rapid inactivation of a calcium-activated potassium channel. *Science* **257**, 1694-1698 (1992).

13. M. Wallner *et al.*, Characterization of and modulation by a beta-subunit of a human maxi KCa channel cloned from myometrium. *Recept Channels* **3**, 185-199 (1995).

14. R. Brenner, T. J. Jegla, A. Wickenden, Y. Liu, R. W. Aldrich, Cloning and functional characterization of novel large conductance calcium-activated potassium channel beta subunits, hKCNMB3 and hKCNMB4. *J. Biol. Chem.* **275**, 6453-6461 (2000).

15. J. Yan, R. W. Aldrich, LRRC26 auxiliary protein allows BK channel activation at resting voltage without calcium. *Nature* **466**, 513-516 (2010).

16. J. Yan, R. W. Aldrich, BK potassium channel modulation by leucine-rich repeat-containing proteins. *Proc Natl Acad Sci U S A* **109**, 7917-7922 (2012).

17. X. Guan, Q. Li, J. Yan, Relationship between auxiliary gamma subunits and mallotoxin on BK channel modulation. *Scientific reports* **7**, 42240 (2017).

18. S. Dudem *et al.*, LINGO1 is a regulatory subunit of large conductance, Ca(2+)-activated potassium channels. *Proc Natl Acad Sci U S A* **117**, 2194-2200 (2020).

19. G. L. Chen, Q.; Yan, J., The leucine-rich repeat domains of BK channel auxiliary γ subunits regulate their expression, trafficking, and channelmodulation functions. *J. Biol. Chem.* **298**, 101664 (2022).

20. Q. Li, X. Guan, K. Yen, J. Zhang, J. Yan, The single transmembrane segment determines the modulatory function of the BK channel auxiliary gamma subunit. *J Gen Physiol* **147**, 337-351 (2016).

21. Q. Li, Fan, F., Kwak, H.R., and Yan, J. , Molecular basis for differential modulation of BK channel voltage-dependent gating by gamma auxiliary subunits. . *J. Gen. Physiol* **145**, 543–554 (2015).

22. G. S. Kallure, K. Pal, Y. Zhou, C. J. Lingle, S. Chowdhury, High-resolution structures illuminate key principles underlying voltage and LRRC26 regulation of Slo1 channels. *bioRxiv* 10.1101/2023.12.20.572542 (2023).

23. D. Yamanouchi, G. Kasuya, K. Nakajo, Y. Kise, O. Nureki, Dual allosteric modulation of voltage and calcium sensitivities of the Slo1-LRRC channel complex. *Mol Cell* **83**, 4555-4569 e4554 (2023).

24. M. Redhardt, S. Raunser, T. Raisch, Cryo-EM structure of the Slo1 potassium channel with the auxiliary gamma1 subunit suggests a mechanism for depolarization-independent activation. *FEBS Lett* **598**, 875-888 (2024).

25. V. Gonzalez-Perez, Xia, X.M., and Lingle C.J. , Functional regulation of BK potassium channels by γ1 auxiliary subunits. *Proc Natl Acad Sci USA* **111**, 4868–4873 (2014).

26. Y. W. Wang, J. P. Ding, X. M. Xia, C. J. Lingle, Consequences of the stoichiometry of Slo1 alpha and auxiliary beta subunits on functional properties of large-conductance Ca2+-activated K+ channels. *J. Neurosci.* **22**, 1550-1561 (2002).

27. K. Nakajo, M. H. Ulbrich, Y. Kubo, E. Y. Isacoff, Stoichiometry of the KCNQ1 - KCNE1 ion channel complex. *Proc Natl Acad Sci U S A* **107**, 18862-18867 (2010).

28. M. Kitazawa, Y. Kubo, K. Nakajo, The stoichiometry and biophysical properties of the Kv4 potassium channel complex with K+ channel-interacting protein (KChIP) subunits are variable, depending on the relative expression level. *The Journal of biological chemistry* **289**, 17597-17609 (2014).

29. J. M. Gonzalez-Perez V , Xia XM, and Lingle CJ, Regulatory γ1 subunits defy symmetry in functional modulation of BK channels. *Proc Natl Acad Sci USA* **115**, 9923-9928 (2018).

30. S. Noda, Y. Suzuki, H. Yamamura, Y. Imaizumi, Single Molecule Fluorescence Imaging Reveals the Stoichiometry of BKgamma1 Subunit in Living HEK293 Cell Expression System. *Biol Pharm Bull* **43**, 1118-1122 (2020).

31. W. Carrasquel-Ursulaez, O. Alvarez, F. Bezanilla, R. Latorre, Determination of the Stoichiometry between alpha- and gamma1 Subunits of the BK Channel Using LRET. *Biophys J* **114**, 2493-2497 (2018).

32. R. S. Hurst, R. A. North, J. P. Adelman, Potassium channel assembly from concatenated subunits: effects of proline substitutions in S4 segments. *Receptors & channels* **3**, 263-272 (1995).

33. C. Fahlke, T. H. Rhodes, R. R. Desai, A. L. George, Jr., Pore stoichiometry of a voltage-gated chloride channel. *Nature* **394**, 687-690 (1998).

34. F. Minier, E. Sigel, Techniques: Use of concatenated subunits for the study of ligand-gated ion channels. *Trends in pharmacological sciences* **25**, 499-503 (2004).

35. M. M. White, Pretty subunits all in a row: using concatenated subunit constructs to force the expression of receptors with defined subunit stoichiometry and spatial arrangement. *Molecular pharmacology* **69**, 407-410 (2006).

36. E. M. Ogielska *et al.*, Cooperative subunit interactions in C-type inactivation of K channels. *Biophys J* **69**, 2449-2457 (1995).

37. N. Zandany, M. Ovadia, I. Orr, O. Yifrach, Direct analysis of cooperativity in multisubunit allosteric proteins. *Proc Natl Acad Sci U S A* **105**, 11697-11702 (2008).

38. W. Wu, A. Gardner, M. C. Sanguinetti, Cooperative subunit interactions mediate fast C-type inactivation of hERG1 K+ channels. *J Physiol* **592**, 4465-4480 (2014).

39. M. Wallner, P. Meera, L. Toro, Determinant for beta-subunit regulation in high-conductance voltage-activated and Ca(2+)-sensitive K+ channels: an additional transmembrane region at the N terminus. *Proc Natl Acad Sci U S A* **93**, 14922-14927 (1996).

40. A. Wei, C. Solaro, C. Lingle, L. Salkoff, Calcium sensitivity of BK-type KCa channels determined by a separable domain. *Neuron* **13**, 671-681 (1994).

41. Y. Y. Chen X, and Aldrich RW, BK channel opening involves side-chain reorientation of multiple deep-pore residues. *Proc. Natl. Acad. Sci. USA* **111**, E79–E88 (2013).

42. X. Y. Wu Y, Wang S, Yi H, Li H, Pan N, Horrigan FT, Wu Y , and Ding J, Intersubunit Coupling in the Pore of BK Channels. *Journal of Biological Chemistry* **284**, 23353–23363 (2009).

43. R. A. Piskorowski, R. W. Aldrich, Relationship between pore occupancy and gating in BK potassium channels. *J Gen Physiol* **127**, 557-576 (2006).

44. J. Yan, Q. Li, R. W. Aldrich, Closed state-coupled C-type inactivation in BK channels. *Proc Natl Acad Sci U S A* **113**, 6991-6996 (2016).

45. L. L. Ken McCormack, Linda E. Iverson, Mark A. Tanouye, and Fred J. Sigworth, Tandem linkage of Shaker K+ channel subunits does not ensure the stoichiometry of expressed channels. *Biophys. J.* **63**, 1406–1411 (1992).

46. O. S. Jon T. Sack, and J. Oliver Dolly, How to Validate a Heteromeric Ion Channel Drug Target: Assessing Proper Expression of Concatenated Subunits. *J. Gen. Physiol.* **131**, 415–420 (2008).

47. Y. Geng *et al.*, BK channels of five different subunit combinations underlie the de novo KCNMA1 G375R channelopathy. *J Gen Physiol* **155** (2023).

48. P. Aryal, M. S. Sansom, S. J. Tucker, Hydrophobic gating in ion channels. *J Mol Biol* **427**, 121-130 (2015).

49. C. M. Wilkens, R. W. Aldrich, State-independent block of BK channels by an intracellular quaternary ammonium. *J Gen Physiol* **128**, 347-364 (2006).

50. J. Thompson, T. Begenisich, Selectivity filter gating in large-conductance Ca(2+)-activated K+ channels. *J Gen Physiol* **139**, 235-244 (2012).

51. Y. Zhou, X. M. Xia, C. J. Lingle, Cysteine scanning and modification reveal major differences between BK channels and Kv channels in the inner pore region. *Proc Natl Acad Sci U S A* **108**, 12161-12166 (2011).

52. G. Yellen, The moving parts of voltage-gated ion channels. *Q Rev Biophys* **31**, 239-295 (1998).

53. M. Kukuljan, P. Labarca, R. Latorre, Molecular determinants of ion conduction and inactivation in K+ channels. *Am J Physiol* **268**, C535-556 (1995).

54. L. G. Cuello, V. Jogini, D. M. Cortes, E. Perozo, Structural mechanism of C-type inactivation in K(+) channels. *Nature* **466**, 203-208 (2010).

55. J. E. Contreras, D. Srikumar, M. Holmgren, Gating at the selectivity filter in cyclic nucleotide-gated channels. *Proc Natl Acad Sci U S A* **105**, 3310-3314 (2008).

56. Y. Yang, Y. Yan, F. J. Sigworth, How does the W434F mutation block current in Shaker potassium channels? *J Gen Physiol* **109**, 779-789 (1997).

57. N. Strutz-Seebohm, U. Henrion, N. Schmitt, E. Schulze-Bahr, G. Seebohm, A common structural component for beta-subunit mediated modulation of slow inactivation in different KV channels. *Cell Physiol Biochem* **31**, 968-980 (2013).

58. W. N. Zagotta, T. Hoshi, R. W. Aldrich, Shaker potassium channel gating. III: Evaluation of kinetic models for activation. *J Gen Physiol* **103**, 321-362 (1994).

59. N. E. Schoppa, F. J. Sigworth, Activation of Shaker potassium channels. III. An activation gating model for wild-type and V2 mutant channels. *J Gen Physiol* **111**, 313-342 (1998).

60. G. Chen, Q. Li, T. I. Webb, M. A. Hollywood, J. Yan, BK channel modulation by positively charged peptides and auxiliary gamma subunits mediated by the Ca2+-bowl site. *J Gen Physiol* **155**, e202213237 (2023).

Figures

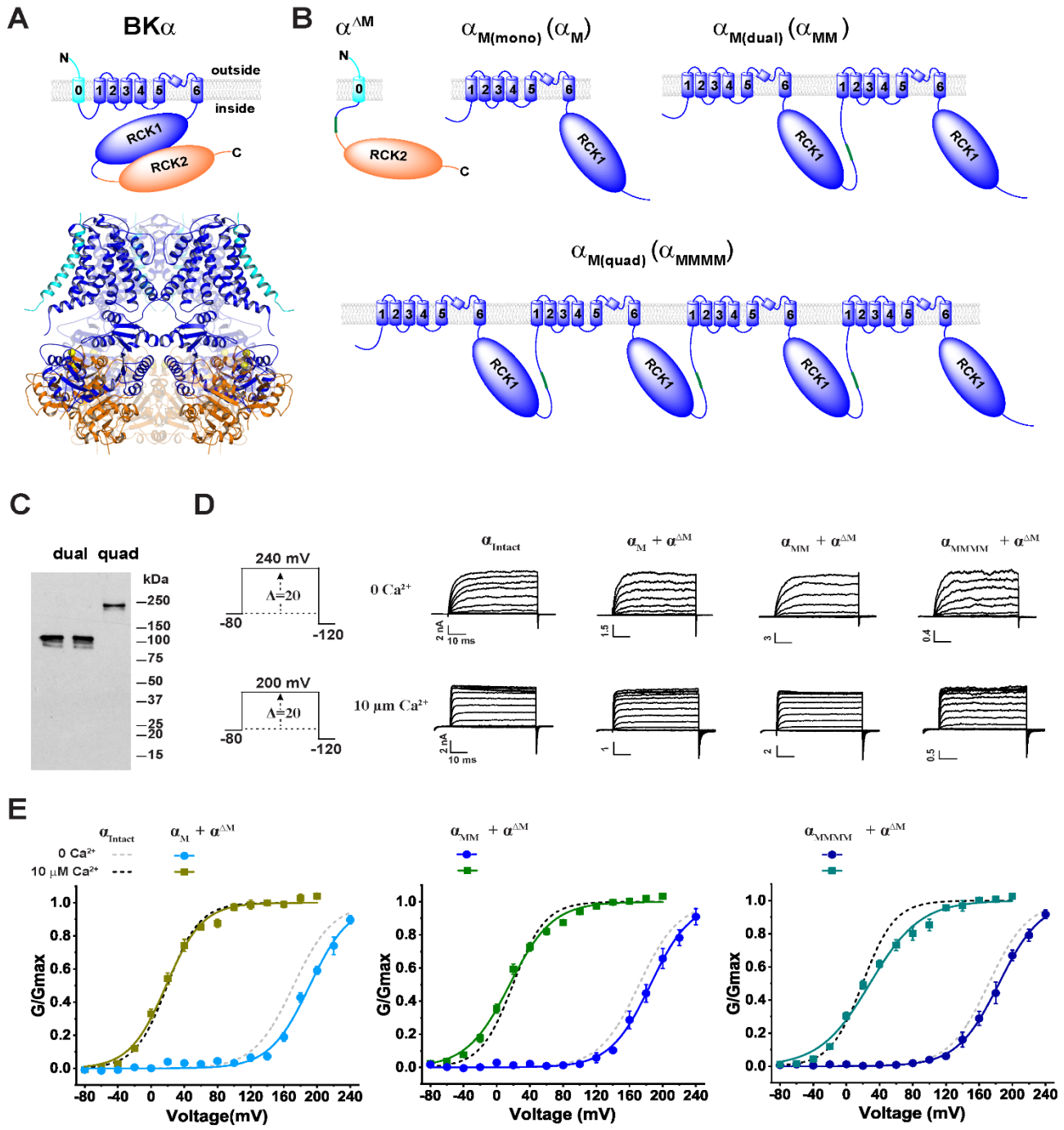

Figure 1. Design of concatenated BKα subunit constructs that form functional channels. (A) Schematic of the membrane topology and side-view of the tetrameric 3D structure of the BKα subunit (PDB ID: 8GHF; cryo-EM structure in plasma membrane (3)) highlighting the three complementary

separable regions in different colors. For clarity, the front and back subunits are shown in a partially transparent mode. **(B)** Schematic of the membrane topology for the BKα_M module, concatenated dual- and quadruple-repeat constructs, and the complementary BK$\alpha^{\Delta M}$ construct. **(C)** Immunoblot analysis of the V5-tagged $\alpha_{M(dual)}$ (left, α_{M1M2}; right, α_{M3M4}) and BK$\alpha_{M(quad)}$ constructs transiently expressed in HEK293 cells with an anti-V5 antibody. (**D**) Representative current traces from BK channels formed by intact, single repeat BKα_M, dual-repeat BK$\alpha_{M(dual)}$, and quadruple-repeat BK$\alpha_{M(quad)}$ constructs in response to membrane depolarization from −80 mV in 20-mV steps at 0 and 10 µM intracellular free Ca^{2+}. **(E)** Voltage dependence of BK channel activation for channels formed by the single (left), dual (middle), and quadruple (right) α_M constructs in the absence and presence of 10 µM Ca^{2+}. Electrophysiological recordings were repeated n = 4 -10, as indicated in Table 1. Error bars represent ± SEM.

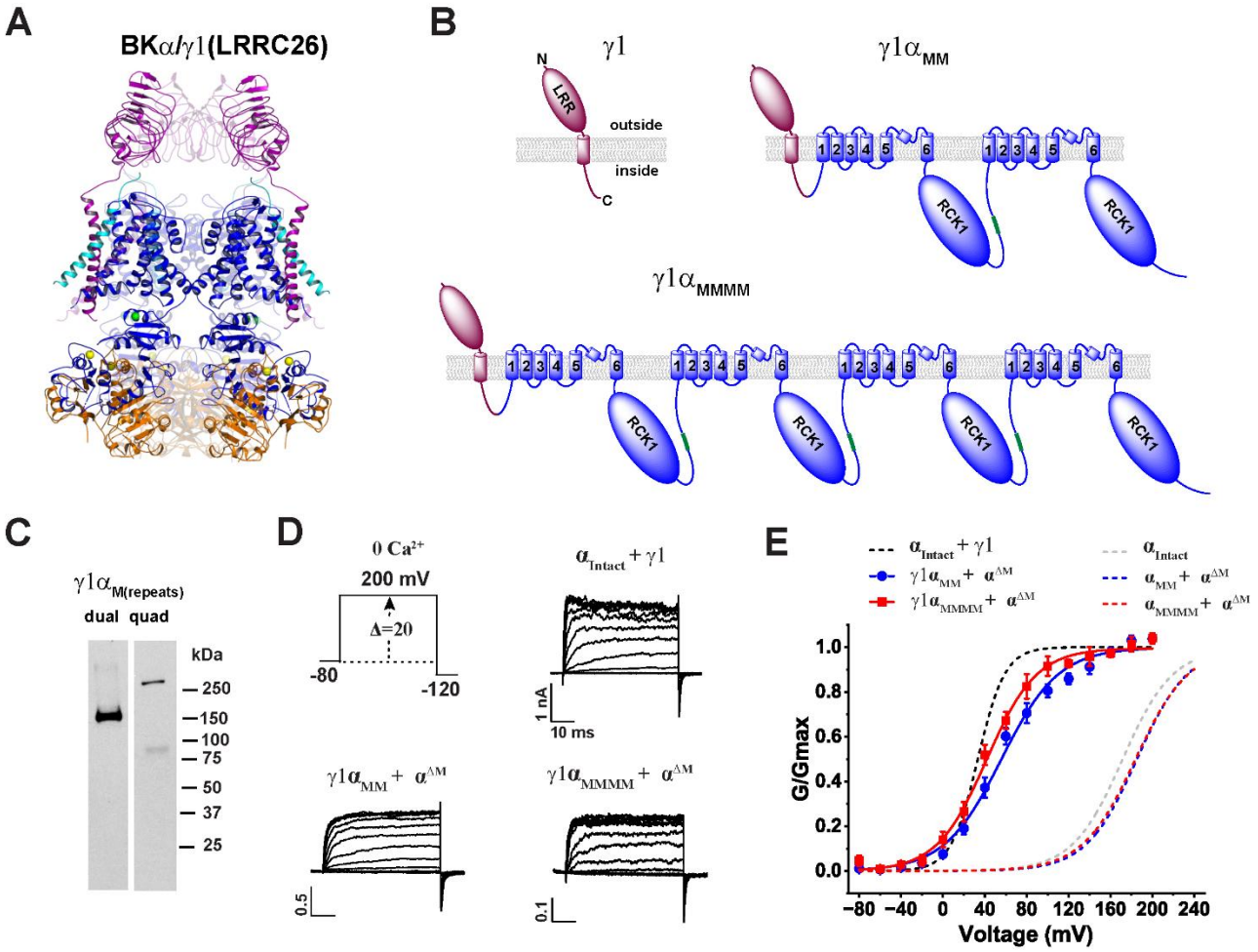

Figure 2. A single γ1 subunit per BK channel is sufficient for full modulation. (A) Side-view of the 3D structure of the BKα/γ1 channel complex (PDB ID: 7YO3 (23)) showing the γ1 subunit in purple and the three separable BKα regions in distinct colors. **(B)** Schematic of the membrane topology for the γ1 subunit and its fusion constructs, created by linking its C-terminus to the N-terminus of the α_M dual- and quadruple-repeat constructs. **(C)** Immunoblot analysis of the V5-tagged $\gamma1\alpha_{M(dual)}$ and $\gamma1\alpha_{M(quad)}$ constructs expressed in HEK293 cells with an anti-V5 antibody. **(D)** Representative current traces from BK channels formed by co-expressing the γ1 subunit with the intact BKα or by γ1-fusion to the concatenated α_M constructs (co-expressed with $\alpha^{\Delta M}$) in response to membrane depolarization from −80 mV in 20-mV steps in the virtual absence of Ca^{2+}. **(E)** Voltage dependence of activation for channels formed by the $\gamma1\alpha_{M(dual)}$ and $\gamma1\alpha_{M(quad)}$ constructs co-expressed with $\alpha^{\Delta M}$. Electrophysiological recordings were repeated n = 5 – 8, as indicated in Table 1. Error bars represent ± SEM.

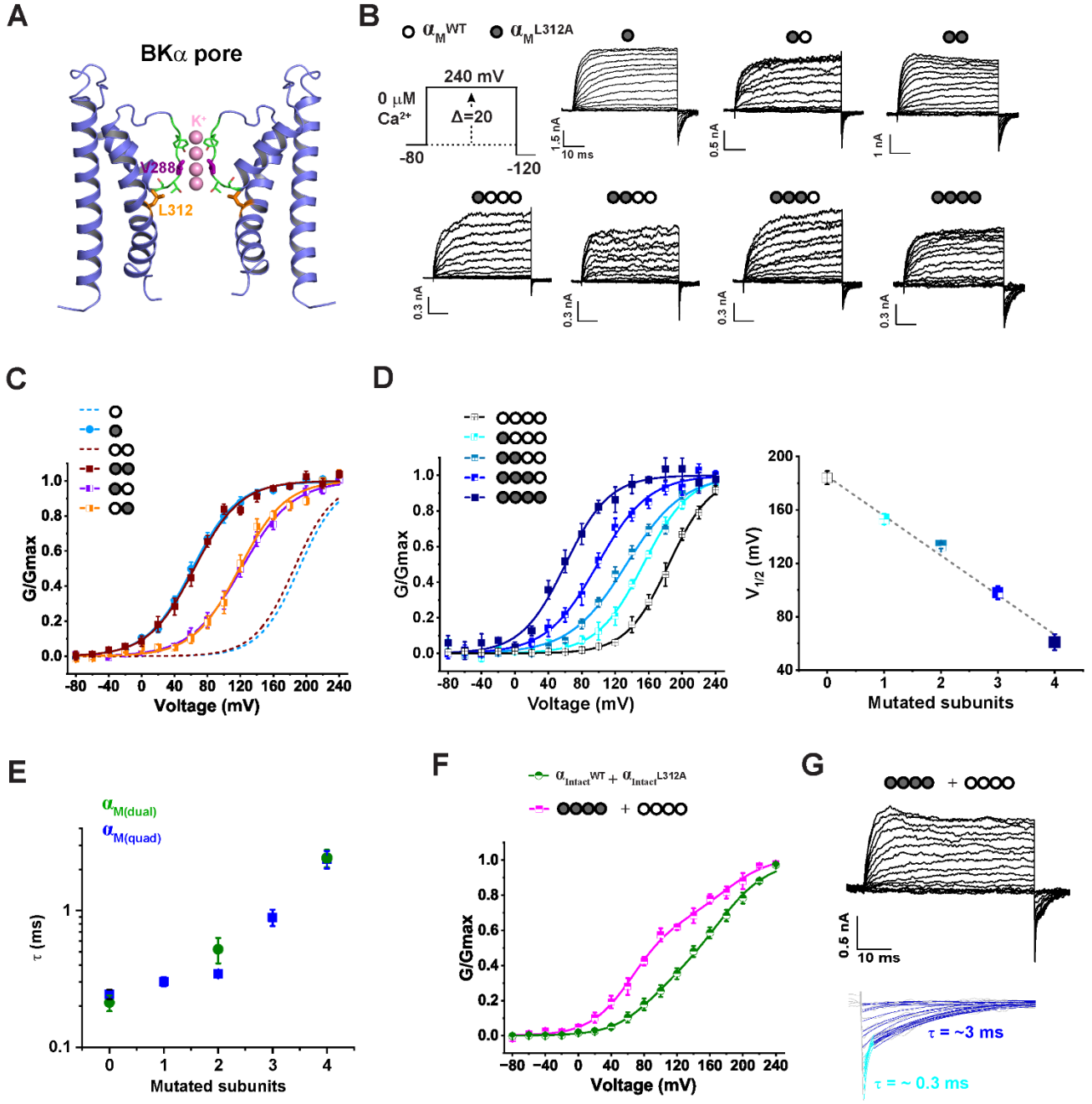

Figure 3. Stoichiometrically incremental effect of the L312A mutation on BK channel voltage gating and validation of functional integrity of the concatenated constructs. (A) Side-view of the BK channel pore structure (PDB ID: 8GHF (3)), highlighting the deep pore residue L312 and selectivity filter residues (stick and line modes). Only two diagonal pore-domains are shown for clarity. **(B)** Representative current traces from BK channels formed by single α_M and concatenated $\alpha_{M(dual)}$ and $\alpha_{M(quad)}$ constructs containing subunit-specific L312A mutations. Depolarizations from −80 mV were applied in 20-mV steps. Mutated

subunits are indicated by filled circles and WT subunits by empty circles. **(C)** Voltage dependence of activation for channels formed by the indicated L312A mutant α_M and $\alpha_{M(dual)}$ constructs co-expressed with $\alpha^{\Delta M}$. Dashed lines show G-V curves of the corresponding non-mutated channels for comparison**. (D)** Voltage dependence of activation for channels formed by the $\alpha_{M(quad)}$ constructs with different numbers of L312A mutations. A plot of the $V_{1/2}$ vs. the number of mutated subunits is shown. **(E)** Plot of tail current decay rates (-120 mV) vs. number of L312A mutations, from $\alpha_{M(dual)}$ and $\alpha_{M(quad)}$ constructs. **(F)** Voltage dependence of activation for channels formed by co-expression of WT and L312A-mutant intact BKα subunits (n = 6), or non-mutated and fully mutated $\alpha_{M(quad)}$ constructs co-expressed with $\alpha^{\Delta M}$. **(G)** Representative current traces from channels formed by co-expressing the non-mutated and fully L312A mutated $\alpha_{M(quad)}$ constructs (co-expressed with $\alpha^{\Delta M}$). Enlarged and fitted tail currents are shown below. Electrophysiological recordings were performed under Ca^{2+}-free conditions and repeated n= 4 -10 as indicated in Table 1. Error bars represent ± SEM.

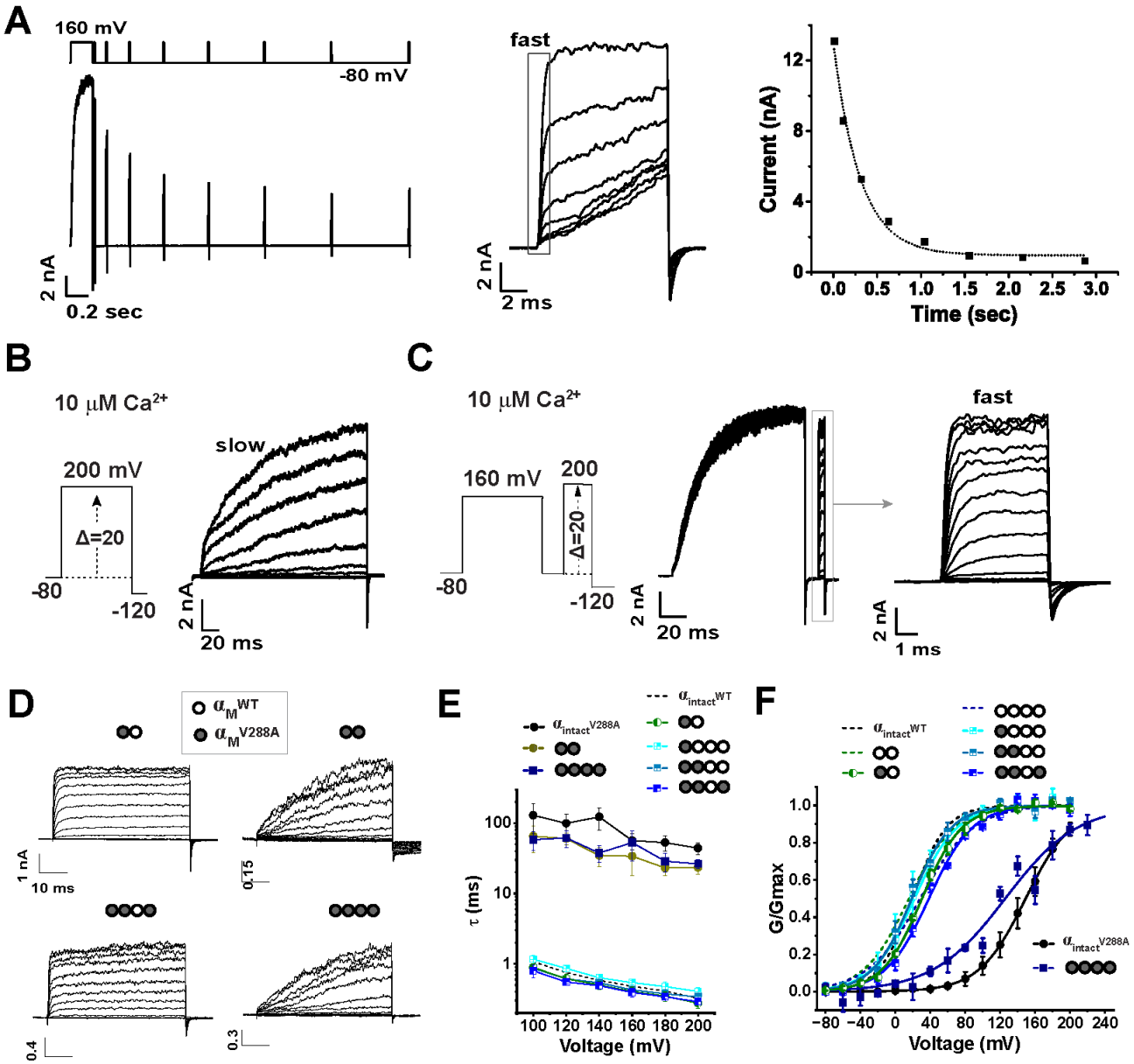

Figure 4. V288A-induced selectivity filter inactivation requires mutation of all subunits. (A) Time-dependent inactivation of V288A-mutant BKα (intact) channels at -80 mV after a prolonged depolarization (160 mV for 200 ms). Inactivation was assayed by monitoring the reduction in fast-activating currents (shown and compared in the middle) elicited by brief depolarization (160 mV for 10 ms) after a prior -80 mV holding time of 10 ms, 0.1 s, 0.2 s, 0.3 s, 0.4 s, 0.5 s, 0.6 s, and 0.7 s. The amplitudes of fast-activating currents are compared (middle) and plotted against time (right). **(B)** Representative current traces of V288A mutant BKα (intact) channels showing slowly developing depolarization-induced currents. **(C)** V288A mutant channel exhibited normal activation gating following

recovery (160 mV for 100 ms) from inactivation, as indicated by currents elicited by brief depolarization to different voltages after brief repolarization. (**D)** Representative current traces from channels formed by concatenated $\alpha_{M(dual)}$ and $\alpha_{M(quad)}$ constructs with subunit-specific V288A mutations (co-expressed with $\alpha^{\Delta M}$). Mutant and WT subunits are indicated as filled and empty circles, respectively. (**E**) Depolarization-induced current development rates for channels formed by non-mutated and V288A-mutant BKα (intact) and concatenated $\alpha_{M(dual)}$ and $\alpha_{M(quad)}$ constructs. Electrophysiological repeats: n = 8 for $\alpha_{(intact)}^{WT}$, 5 for $\alpha_{(intact)}^{V288A}$, 4 for $\alpha_M^{V288A}{}_M^{WT}$, 4 for $\alpha_M^{V288A}{}_M^{V288A}$, 4 for $\alpha_M^{V288A}{}_M^{WT}{}_M^{WT}{}_M^{WT}$, 4 for $\alpha_M^{V288A}{}_M^{V288A}{}_M^{WT}{}_M^{WT}$, 3 for $\alpha_M^{V288A}{}_M^{V288A}{}_M^{WT}{}_M^{V288A}$, and 4 for $\alpha_M^{V288A}{}_M^{V288A}{}_M^{V288A}{}_M^{V288A}$. (**F**) Voltage dependence of depolarization-induced currents for BK channels formed by non-mutated and V288A-mutant BKα (intact) and concatenated $\alpha_{M(dual)}$ and $\alpha_{M(quad)}$ constructs. Electrophysiological repeats n= 3-5 as indicated in Table 1. All recordings were performed using symmetric K^+ (140 mM) solutions with 10 μM intracellular Ca^{2+}. Error bars represent ± SEM.

Figure supplement legends

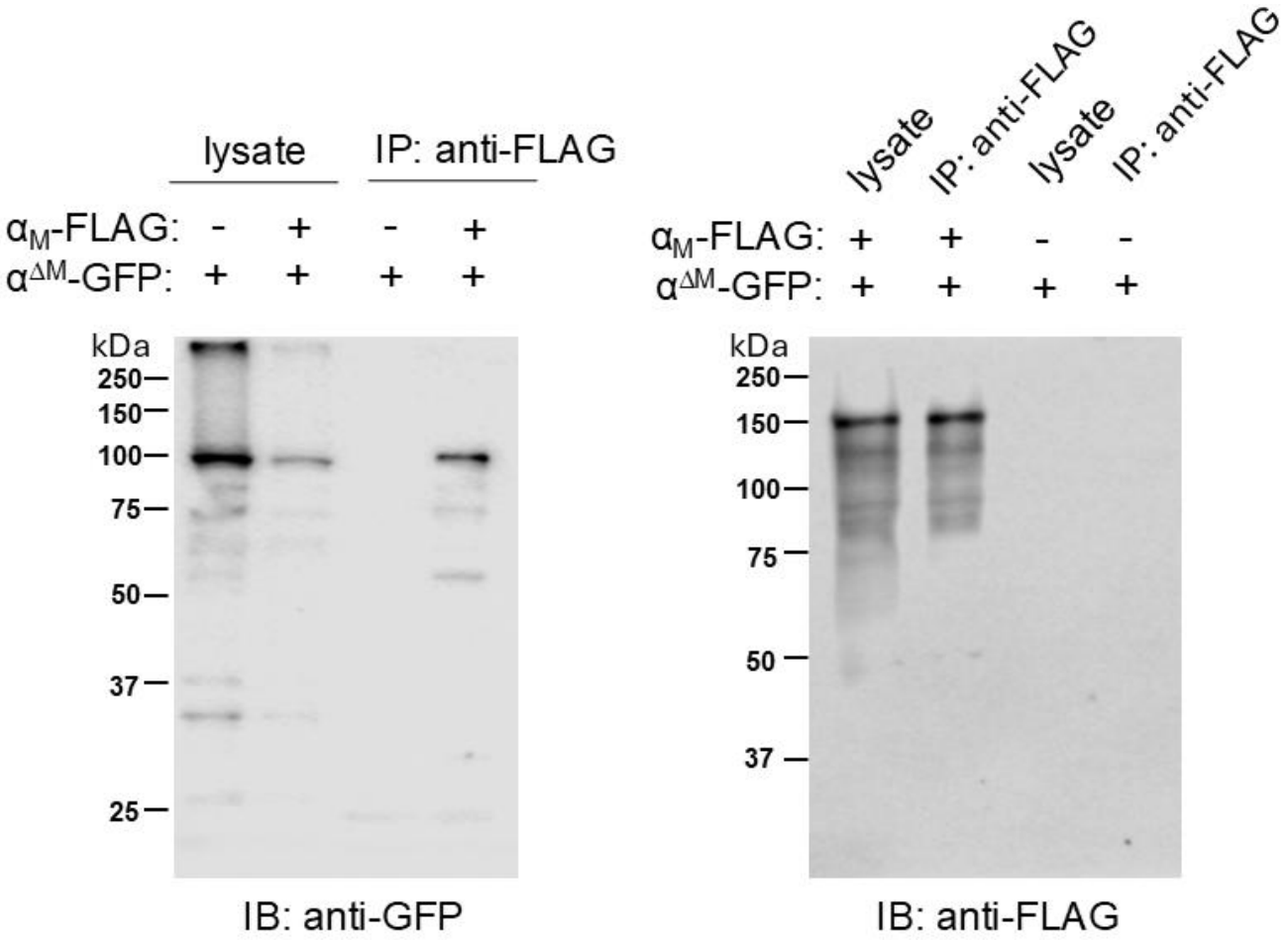

Figure 1 - figure supplement 1. Complex formation between split BKα subunit constructs. A FLAG-tagged αM construct was co-expressed with GFP-tagged αΔM or an empty vector in HEK293 cells. For comparison, equal amounts of total cellular protein from cell lysates were loaded onto SDS–PAGE. Notably, the presence of α_M caused a reduction of the $\alpha^{\Delta M}$ expression and the singular α_M construct mostly oligomerized on SDS-PAGE.

Table 1 Boltzmann-fit parameters of the voltage-dependent concatenated tandem BK channel activation in the wildtype, mutants in the absence and presence of intracellular Ca^{2+}.

Expression*	Ca^{2+} (μM)	Boltzmann fit parameters		
		$V_{1/2}$ (mV)	z	n§
α_{intact}	0	172 ± 2	1.08 ± 0.04	9
α_{intact}	10	19 ± 4	1.47 ±0.10	8
α_{M}	0	191 ± 1	1.11 ± 0.13	4
α_{M}	10	18 ± 3	1.20 ± 0.06	6
α_{MM}	0	186 ± 5	1.12 ± 0.12	5
α_{MM}	10	16 ± 3	1.02 ± 0.03	10
α_{MMMM}	0	184 ± 5	1.09 ± 0.07	6
α_{MMMM}	10	29 ± 4	0.86 ± 0.06	4
$\alpha_{intact} + \gamma 1$	0	35 ± 2	1.56 ± 0.11	8
$\gamma 1 \alpha_{MM}$	0	56 ± 4	0.99 ± 0.07	6
$\gamma 1 \alpha_{MMMM}$	0	42 ± 3	1.13 ± 0.13	5
α_{M}^{L312A}	0	62 ± 4	0.96 ± 0.07	6
$\alpha_{M}^{L312A}{}_{M}^{WT}$	0	121 ± 6	0.90 ± 0.04	10
$\alpha_{M}^{WT}{}_{M}^{L312A}$	0	118 ± 5	0.95 ± 0.07	4
$\alpha_{M}^{L312A}{}_{M}^{L312A}$	0	64 ± 5	0.97 ± 0.08	5
$\alpha_{M}^{L312A}{}_{M2}^{WT}{}_{M3}^{WT}{}_{M4}^{WT}$	0	153 ± 4	0.96 ± 0.10	5
$\alpha_{M}^{L312A}{}_{M}^{L312A}{}_{M}^{WT}{}_{M}^{WT}$	0	133 ± 2	0.77 ± 0.05	4
$\alpha_{M}^{L312A}{}_{M}^{L312A}{}_{M}^{L312A}{}_{M}^{WT}$	0	98 ± 5	0.90 ± 0.11	5
$\alpha_{M}^{L312A}{}_{M}^{L312A}{}_{M}^{L312A}{}_{M}^{L312A}$	0	61 ± 6	1.05 ± 0.09	5
$\alpha_{M}^{L312A}{}_{M}^{L312A}{}_{M}^{L312A}{}_{M}^{L312A} + \alpha_{M}^{WT}{}_{M}^{WT}{}_{M}^{WT}{}_{M}^{WT}$	10	180 ± 13 (36%) 65 ± 8 (64%)	0.90 ± 0.52 1.01 ± 0.13	5
α_{intact}^{V288A}	10	149 ± 8	1.06 ± 0.10	5
$\alpha_{M}^{V288A}{}_{M}^{WT}$	10	31 ± 2	1.14 ± 0.09	5
$\alpha_{M}^{V288A}{}_{M}^{WT}{}_{M}^{WT}{}_{M}^{WT}$	10	21 ± 11	1.16 ± 0.06	3
$\alpha_{M}^{V288A}{}_{M}^{V288A}{}_{M}^{WT}{}_{M}^{WT}$	10	19 ± 2	1.19 ± 0.17	3
$\alpha_{M}^{V288A}{}_{M}^{V288A}{}_{M}^{WT}{}_{M}^{V288A}$	10	38 ± 3	1.05 ± 0.06	3

$\alpha_M^{V288A}{}_M^{V288A}{}_M^{V288A}{}_M^{V288A}$	10	127 ± 10	0.75 ± 0.21	3

[*] Except the full-length BKα_{intact} construct, all other listed (derivatives of α_M) constructs were co-expressed with the complementary $\alpha^{\Delta M}$-GFP construct.

[§] The number of recorded excised inside-out patches from different HEK293 cells.